EBioMedicine 39 (2019) 484–496

Contents lists available at ScienceDirect

EBioMedicine

journal homepage: www.ebiomedicine.com

EBioMedicine
Published by THE LANCET

Research paper

Reversion of *in vivo* fibrogenesis by novel chromone scaffolds

Han-Soo Kim [a,b], Young-Min Yoon [c], Moon Kee Meang [c,d], Yae Eun Park [e,f], Ji Yong Lee [g], Tae Hee Lee [h], Ji Eun Lee [e], Ik-Hwan Kim [d], Byung-Soo Youn [c,*]

[a] Department of Biomedical Sciences, Catholic Kwandong University College of Medicine, Gangneung-si, Gangwon-do 25601, Republic of Korea
[b] Basic Research Division, Biomedical Institute of Mycological Resource, College of Medicine,Catholic Kwandong University, Gangneung-si, Gangwon-do, 25601, Republic of Korea
[c] OsteoNeuroGenInc, Seoul 08501, Republic of Korea
[d] Department of Biotechnology, Korea University, Seoul 02841, Republic of Korea
[e] Center for Theragnosis, Biomedical Research Institute, Korean Institute of Science and Technology, Department of Biochemistry, College of Life Science and Biotechnology, Yonsei University, Seoul 03722, Republic of Korea
[f] College of Life Science and Biotechnology, Yonsei University, Seoul 03722, Republic of Korea
[g] Department of Anatomy, Yonsei University Wonju College of Medicine, Wonju-si, Gangwon-do 26426, Republic of Korea
[h] School of Oriental Medicine, Formulae Pharmacology Department, Gachon University, Seongnam-si 13120, Republic of Korea

ARTICLE INFO

Article history:
Received 3 July 2018
Received in revised form 10 December 2018
Accepted 10 December 2018
Available online 2 January 2019

Keywords:
Chromone scaffold
Epithelial–mesenchymal transition
Stem cells
Idiopathic pulmonary fibrosis
Myofibroblasts
Dedifferentiation

ABSTRACT

Background: Myofibroblasts are known to play a key role in the development of idiopathic pulmonary fibrosis (IPF). Two drugs, pirfenidone and nintedanib, are the only approved therapeutic options for IPF, but their applications are limited due to their side effects. Thus, curative IPF drugs represent a huge unmet medical need.
Methods: A mouse hepatic stellate cell (HSC) line was established that could robustly differentiate into myofibroblasts upon treatment with TGF-β. Eupatilin was assessed in diseased human lung fibroblasts from IPF patients (DHLFs) as well as in human lung epithelial cells (HLECs). The drug's performance was extensively tested in a bleomycin-induced lung fibrosis model (BLM). Global gene expression studies and proteome analysis were performed.
Findings: Eupatilin attenuated disease severity of BLM in both preventative and therapeutic studies. The drug inhibited the *in vitro* transdifferantiation of DHLFs to myofibroblasts upon stimulation with TGF-β. No such induction of the *in vitro* transdifferantiation was observed in TGF-β treated HLECs. Specific carbons of eupatilin were essential for its anti-fibrotic activity. Eupatilin was capable of dismantling latent TGF-β complex, specifically by eliminating expression of the latent TGF-β binding protein 1 (LTBP1), in ECM upon actin depolymerization. Unlike eupatilin, pirfenidone was unable to block fibrosis of DHLFs or HSCs stimulated with TGF-β. Eupatilin attenuated phosphorylation of Smad3 by TGF-β. Eupatilin induced myofibroblasts to dedifferentiate into intermediate HCS-like cells.
Interpretation: Eupatilin may act directly on pathogenic myofibroblasts, disarming them, whereas the anti-fibrotic effect of pirfenidone may be indirect. Eupatilin could increase the efficacy of IPF treatment to curative levels.

1. Introduction

Fibrosis is a complex disease state in which elevated proliferation of myofibroblasts is accompanied by overproduction of extracellular matrix (ECM) components [1]. The transdifferentiation of fibroblasts into myofibroblasts plays a central role in perpetuating the fibrotic process [2] in which TGF-β is a key modulator of the fibrogenesis [3]. Which cell types produce TGF-β in the lung niches remains to be elucidated [4]. Binding of TGF-β to TGFR is meticulously regulated by formation of latent TGF-β complex as a cargo proteome comprising heterodimeric integrins (largely integrin αvβ3), the tripeptide Arg-Gly-Asp (RGD), the chemically modified lamina-associated polypeptide 1 (LAP1), and LTBP1 or LTBP4 [5] in the ECM. Selective intervention in the formation of latent TGF-β complex represents a novel strategy for anti-IPF therapy.

Two fibrotic diseases, idiopathic pulmonary fibrosis (IPF) and liver fibrosis preceded by non-alcoholic steatohepatitis (NASH), affect many people around the world, and effective therapies against these conditions are urgently required. However, no curative drugs for these conditions are yet available [6,7]. Two small-molecule anti-fibrotic

Abbreviations: CS, chromone scaffold; CD, chromone scaffold derivative; IPF, idiopathic pulmonary fibrosis; BLM, bleomycin-induced lung fibrosis model; NASH, non-alcoholic steatohepatitis; DHLF, diseased human lung fibroblast.

* Corresponding author at: OsteoNeuroGen, Inc. Ace High-end Tower 9th 233, Gasandigital-1-ro, Geumcheon-gu, Seoul 08501, Republic of Korea.
E-mail address: byung4jc@gmail.com (B.-S. Youn).

https://doi.org/10.1016/j.ebiom.2018.12.017

Reseach in context

Evidence before this study

Natural compounds containing a chromone scaffold (CS) have not been assessed for anti-fibrotic capacity, nor has the use of synthetic CS compounds been investigated in this context. The two currently FDA-approved drugs for fibrotic diseases, pirfenidone and nintedanib, are not curative. The demand for curative anti-IPF drugs represents a major unmet medical need. The mechanism of action (MOA) of pirfenidone remains elusive. MOA(s) of eupatilin remains to be elucidated.

Added value of this study

This study presents a strong candidate drug with novel MOA (s) that could substantially improve anti-IPF efficacy with significantly lower toxicity. In contrast to pirfenidone, eupatilin most likely acts on pathogenic myofibroblasts, resulting in actin depolymerization followed by dismantling of latent TGF-β complex; this process disarms TGF-β receptor (TGFR) signaling and cripples the induction of the epithelial–mesenchymal transition (EMT), another term for fibrogenesis. In addition, eupatilin may cause dedifferentiation of myofibroblasts into some intermediate cell types, resembling translational observations in human patients recovering from liver fibrosis. In studies using human primary lung fibroblasts and a mouse HSC cell line, we identified shared gene expression signatures between lung and liver fibrosis following stimulation with TGF-β.

Implications of all the available evidence

Taken together, the CS-containing natural compounds exemplified by eupatilin and their synthetic analogues represent a new line of curative anti-IPF drugs for use in monotherapy. Furthermore, in conjunction with pirfenidone or nintedanib, the anti-fibrotic effects of these drugs could substantially improve the efficacy of IPF therapy.

drugs, pirfenidone (Esbriet) and nintedanib (Ofev), have recently been approved for IPF [8], but to successfully treat this disease, their efficacies must be improved and their side effects ameliorated. Nintedanib is an angiokinase inhibitor, whereas the mechanisms underlying the anti-fibrotic activities of pirfenidone remain to be elucidated [9,10].

The flavones, members of the polyphenol family, include >10,000 compounds generated by various plant species [11]. In general, these phytochemicals play important roles in plant growth, development, protection from radiation damage, and defense against natural enemies [12–14]. Due to their anti-oxidant and anti-inflammatory potentials, flavones have long been used to treat inflammatory diseases such as arthritis and asthma [15]. Chromone, 1,4-benzopyrone-4-one, is a central chemical scaffold in flavones [16], and chromone derivatives (CDs) are a diverse family of compounds in which branching chemical residues are coupled to this core chemical framework [17]. We recently reported that eupatilin, a CD from an *Artemisia* species, dramatically inhibited osteoclastogenesis *via* actin depolymerization in cells differentiated from bone marrow–derived macrophages in the presence of macrophage-colony stimulating factor (M-CSF) and receptor activator of nuclear factor kappa-B ligand (RANKL) [18], and a vast majority of the downregulated genes associated with the epithelial mesenchymal transition (EMT), which is a hallmark of fibrosis. Specifically, 24 of the 50 top genes differentially regulated by eupatilin during osteoclastogenesis are associated with EMT, prompting us to hypothesize that eupatilin could prevent fibrosis (Fig. S1).

Here, we show that eupatilin acts directly on pathogenic myofibroblasts stimulated with TGF-β, stimulating rapid actin depolymerization, leading to dismantling of latent TGF-β complex followed by near-complete inhibition of induction of multiple EMT genes. At the same time, eupatilin blocks phosphorylation of Smad3 and may be able to dedifferentiate myofibroblasts into intermediate cell types, thereby reversing fibrosis. These combined therapeutic effects, which are distinct from those of pirfenidone, ameliorate lung fibrosis. This observation opens the door to development of a powerful therapeutic modality against IPF.

2. Materials and methods

2.1. Cell culture and reagents

DHLFs were purchased from Lonza (Basel, Switzerland) and cultured in fibroblast growth medium (FBM, Lonza, Walkersville, MD, USA). Recombinant human TGF-β and PDGF were obtained from Peprotech (Rocky Hill, CT, USA) and used at a final concentration of 5 ng/ml. Chemically synthesized eupatilin was obtained from Syngene International Ltd. (Bangalore, India), dissolved at a stock concentration of 50 mM in DMSO, and stored in aliquots at −20 °C. DMSO at 0.1% (v/v) was used as a control. ONGE200 (hispidulin) and ONGA300 (jaceosidin) were purchased from AK Scientific (Union City, CA, USA). The remaining 32 CDs in the test set were purchased from Analyticon (Berlin, Germany). For simultaneous treatment, ONGHEPA1 cells (5.5×10^4 cells/well in 1 ml) were seeded in 24-well plates. The anti-fibrotic effect of eupatilin was examined under a microscope (EVOS, Life Technologies, Carlsbad, CA, USA).

2.2. Flow cytometry

Cell pellets were suspended in PBS supplemented with 1% FBS and stained with antibodies against CD29, CD44, CD45, CD71, CD90, CD106, and CD117. All antibodies were obtained from BD Biosciences (San Jose, CA, USA). Labeled cells were analyzed on a flow cytometer (FC500, Beckman Coulter, Fullerton, CA, USA).

2.3. Cell viability assay

Cells were treated with TGF-β and the indicated concentrations of eupatilin (or other CDs) for 24 h. Cell viability was measured using the CCK-8 kit (Dojindo Molecular Technologies, Tokyo, Japan).

2.4. Immunostaining

For immunofluorescence staining, ONGHEPA1 cells were grown on 8-well glass chamber slides (LabTek II, Thermo Fisher, Rochester, NY, USA) and fixed with methanol at −80 °C for 2 h. After washing with PBS, cells were blocked and permeabilized by incubation at room temperature for 2 h in PBS/5% FBS with 0.1% Triton X-100. After incubation with primary antibodies at 4 °C overnight, cells were washed, stained with dye-conjugated secondary antibodies, and incubated at room temperature for 2 h. GATA4 (Santa Cruz Biotechnology, Dallas, TX, USA) and cytokeratin 18 (Santa Cruz Biotechnology) were used as markers of endoderm and endothelial cells, respectively. Nuclei were counterstained with DAPI.

2.5. Reverse transcriptase PCR and real-time PCR

Cells cultured in 24-well plates were harvested with trypsin-EDTA solution (Welgene, Seoul, Korea). Total RNA was purified from the pellets using the RNeasy Mini Kit (Qiagen, Valencia, CA, USA). RNA was

reverse-transcribed using the cDNA Synthesis Kit (PCR Biosystems, London, United Kingdom). Synthesized cDNA was amplified with StepOne Plus (Applied Biosystems, Life Technologies) and 2× qPCRBio Probe Mix Hi-ROX (PCR Biosystems). Comparisons between mRNA levels were performed using the ΔΔCt method, with *Gapdh* as the internal control.

2.6. RNA-seq processing, differential gene expression analysis, and interactome analysis

Processed reads were mapped to the *Mus musculus* reference genome (Ensembl 77) using Tophat and Cufflink with default parameters [19]. Differential analysis was performed using Cuffdiff [19] using default parameters. Further, FPKM values from Cuffdiff were normalized and quantitated using the R Package Tag Count Comparison (TCC) [20] to determine statistical significance (*e.g.*, *p*-values) and differential expression (*e.g.*, fold changes). Gene expression values were plotted in various ways (*i.e.*, Scatter, MA, and Volcano plots), using fold-change values, using an R script developed in-house. The protein interaction transfer procedure was performed using the STRING database [21] with the differentially expressed genes. A total of 60 Gb of sequence was generated, and 10,020 transcripts were read and compared. The highest-confidence interaction score (0.9) was applied from the *Mus musculus* species and information about interaction was obtained from text mining, experiments, and databases (http://www.string-db.org/).

2.7. Ethic statement

The animal study was conducted at Syngene International (Bangalore, India) (IAEC No. Syngene/IAEC/GLP/C-094/2016–2019) in compliance with the guidelines of the Committee for the Purpose of Control and Supervision of Experiments on Animals (CPCSEA) of the Government of India and Woojung BSC (Seoul, Korea) under IRB 13023.

2.8. Bleomycin-induced lung fibrosis model

C57BL/6 J mice were anesthetized by inhalation of 70% N_2O and 30% O_2 gas containing 1.5% isoflurane. Bleomycin (BLM) solution (0.03 U in 50 μl of saline) in distilled water was directly injected into the lungs, all at once, using a visual instillobot. Immediately after injection, the mice were allowed to recover from the anesthetic, and then housed in normal cages. Twelve days after the administration of BLM, eupatilin was forcibly nasally administered *via* a micropipette, once a day (five times a week) for 1 week. Eupatilin was dissolved in DPBS buffer (containing 1% DMSO), and 1 ml/kg was administered based on the most recent body weight. For 2 to 3 days after administration of eupatilin, mice were monitored for toxic symptoms or death, but no abnormal symptoms were observed. Three mice per test group were selected, and their lung tissues were excised. Lung tissues were stained with Masson's trichrome and observed under a microscope. Results were expressed as mean values and standard deviations. One hour before sacrifice, a final dose of eupatilin or pirfenidone was administered for plasma or lung pharmacokinetics (PKs). The bleomycin-treated mice exhibited a rapid decline in weight, but the sham control behaved normally. Eupatilin- or pirfenidone-administered mice exhibited weight gain from day 3 onward. Control and eupatilin-treated mice data were compared using Student's *t*-test. Differences between samples were considered statistically significant when $p < 0.05$.

2.9. Plasma, liver, and lung bioavailability of eupatilin and pirfenidone in mice

To evaluate the plasma, liver, and lung tissue bioavailability of eupatilin or pirfenidone in mice (C57BL/6), a single oral dose of drug in 0.5% CMC and 1% Tween 80 was administered, and the PKs were examined at early time points (5 min, 15 min, 30 min, 1 h, or 2 h) as post oral dose of each 100 mpk. Samples were analyzed for eupatilin and its glucuronide using an API 6500 (SciEx/IET, Mundelein, IL, USA) after a brief non-GLP method development. Concentration in plasma, liver, and lung tissue (PK) was compared.

2.10. Proteomic analysis of ONGHEPA1 cells stimulated with TGF-β or TGF-β plus eupatilin

ONGHEPA1 cells stimulated with TGF-β or TGF-β plus eupatilin were lysed in modified RIPA buffer (150 mM NaCl, 1% Triton X-100, 0.5% deoxycholate, 0.2% SDS, 1 mM EDTA, 50 mM Tris-HCl, pH 7.5, and protease inhibitor cocktail), and protein concentrations were determined using the bicinchoninic acid (BCA) method. Cell lysate (80 μg/sample) was subjected to electrophoresis on a NuPAGE gel (4–12% Bis-Tris gel, Invitrogen, Carlsbad, CA, USA) prior to mass spectral analysis. For each condition, three replicates were run on the same gel, and the gels were stained with Coomassie Brilliant Blue R-250 (Sigma-Aldrich Korea, Seoul, Korea). The stained gel for each cell lysate sample was divided into 17 slices, and each excised gel piece was transferred to a microcentrifuge tube (Eppendorf AG, Hamburg, Germany). Proteins were digested in-gel with trypsin and subjected to nanocapillary coupled to an LTQ XL-Orbitrap mass spectrometer (Thermo Fisher Scientific, Waltham, MA, USA). Each LC-MS/MS file was analyzed using the SEQUEST algorithm in Proteome Discoverer 1.4 (Thermo Fisher Scientific). MS and MS/MS data were searched against the SwissProt human database (April 2017) with 20,198. The search criteria were set to a mass tolerance of 15 ppm for MS data and 0.5 Da for MS/MS data, with fixed modification of carbamidomethylation of cysteine (+57.021 Da) and variable modification of methionine oxidation (+15.995 Da). A strict false discovery rate of 0.01, relaxed false discovery rate of 0.05, and total of two target values for a decoy database search were applied. All proteins were identified by two or more unique peptides. The relative abundances of proteins identified from the two cell types were calculated based on normalized spectral abundance factor (NSAF). The spectral count data (*i.e.*, the number of MS/MS spectra matched to a protein) were first extracted using the Proteome Discoverer 1.4 software (Thermo Scientific Inc., San Jose, CA, USA), and then exported to Microsoft Excel. Then, NSAF for each protein was calculated as follows:

$$(\mathrm{NSAF})_k = \frac{(\mathrm{SpC}/L)_k}{\sum_{i=1}^{N} (\mathrm{SpC}/L)_i}$$

in which the total number of MS/MS spectra matching peptides from protein *k* (SpC) was divided by the protein's length (*L*) and then divided by the sum of SpC/*L* for all *N* proteins. Prior to calculation of NSAF, the proteins identified for the replicates of each sample set were first filtered using two criteria: proteins with total spectral count (the number of MS/MS spectra matched to the protein) ≥6, which were present in all three replicates in at least each sample set, were considered to be reproducibly identified and were retained for quantitative analysis. Then, a value of 0.5 was added to all spectral counts to compensate for null values and enable calculation of fold changes between the two cell types even when a protein was absent or below the limit of detection. For statistical analysis of the dataset, the natural logarithm of each NSAF value was calculated, followed by Student's *t*-test comparison of the ln(NSAF) values obtained from the three replicates of each cell lysate. The resulting *p*-value <.05 was considered statistically significant.

3. Results

3.1. Specific carbons of the CS and linked functional groups are critical for anti-fibrotic effects

The chromone scaffold (CS) of eupatilin, indicated by the highlighted carbons in Fig. 1a, is linked to a phenyl ring coupled to two methoxy

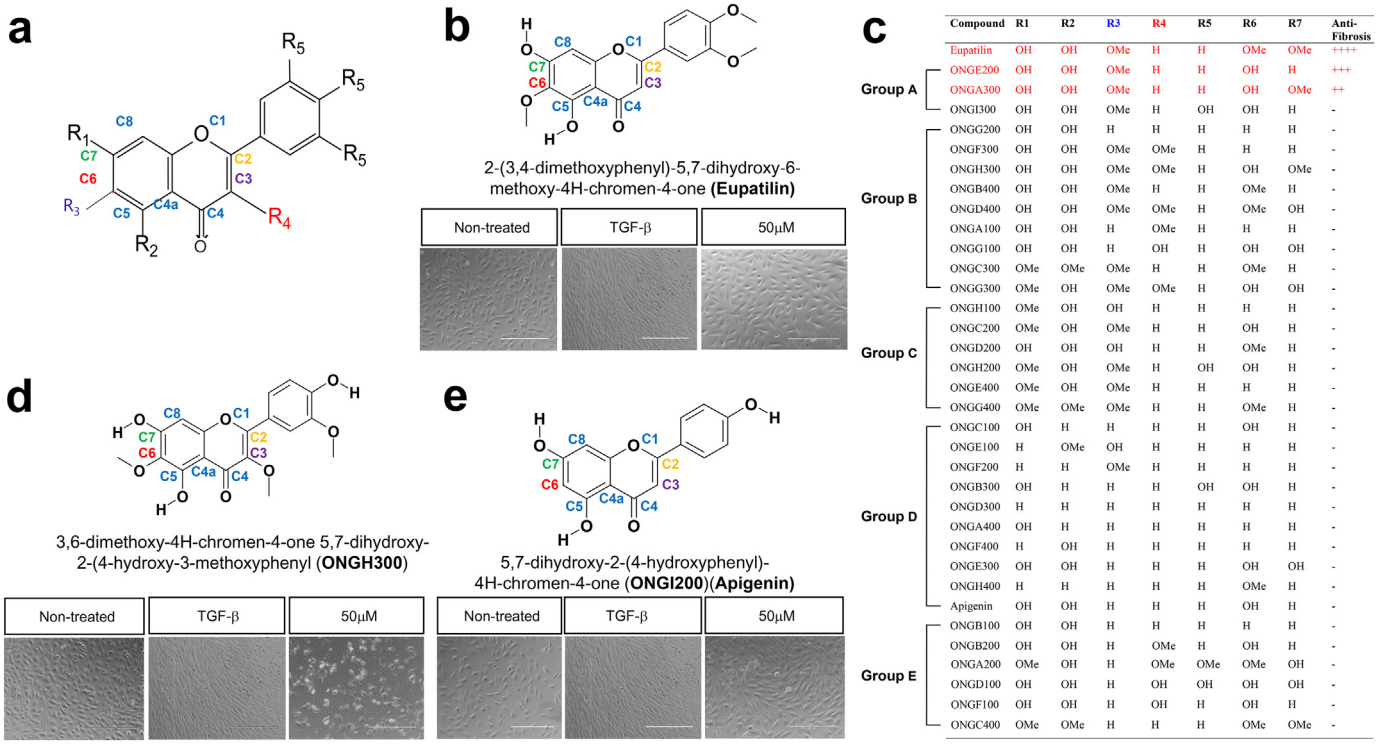

	Compound	R1	R2	R3	R4	R5	R6	R7	Anti-Fibrosis
	Eupatilin	OH	OH	OMe	H	H	OMe	OMe	++++
Group A	ONGE200	OH	OH	OMe	H	H	OH	H	+++
	ONGA300	OH	OH	OMe	H	H	OH	OMe	++
	ONGI300	OH	OH	OMe	H	OH	OH	H	-
Group B	ONGG200	OH	OH	H	H	H	H	H	-
	ONGF300	OH	OH	OMe	OMe	H	H	H	-
	ONGH300	OH	OH	OMe	OMe	H	OH	OMe	-
	ONGB400	OH	OH	OMe	H	H	OMe	H	-
	ONGD400	OH	OH	OMe	OMe	H	OMe	OH	-
	ONGA100	OH	OH	H	OMe	H	H	H	-
	ONGG100	OH	OH	H	OH	H	OH	OH	-
	ONGC300	OMe	OMe	OMe	H	H	OMe	H	-
	ONGG300	OMe	OH	OMe	OMe	H	OH	OH	-
Group C	ONGH100	OMe	OH	OH	H	H	H	H	-
	ONGC200	OMe	OH	OMe	H	H	OH	H	-
	ONGD200	OH	OH	OH	H	H	OMe	H	-
	ONGH200	OMe	OH	OMe	H	OH	OH	H	-
	ONGE400	OMe	OH	OMe	H	H	H	H	-
	ONGG400	OMe	OMe	OMe	H	H	OMe	H	-
Group D	ONGC100	OH	H	H	H	H	OH	H	-
	ONGE100	H	OMe	OH	H	H	H	H	-
	ONGF200	H	H	OMe	H	H	H	H	-
	ONGB300	OH	H	H	H	OH	OH	H	-
	ONGD300	H	H	H	H	H	H	H	-
	ONGA400	OH	H	H	H	H	H	H	-
	ONGF400	H	OH	H	H	H	H	H	-
	ONGE300	OH	OH	H	H	H	OH	OH	-
	ONGH400	H	H	H	H	H	OMe	H	-
	Apigenin	OH	OH	H	H	H	OH	H	-
Group E	ONGB100	OH	OH	H	H	H	H	H	-
	ONGB200	OH	OH	H	OMe	H	OH	H	-
	ONGA200	OMe	OH	H	OMe	OMe	OMe	OH	-
	ONGD100	OH	OH	H	OH	OH	OH	OH	-
	ONGF100	OH	OH	H	OH	H	OH	H	-
	ONGC400	OMe	OMe	H	H	H	OMe	OMe	-

Fig. 1. Structure–activity relationship of a selected group of chromone derivatives. (a) Chemical structure of the general chromone scaffold, with its carbons denoted in colored fonts. C2, C3, C6, and C7 are critical for anti-fibrogenesis. (b) ONGHEPA1 cells were simultaneously stimulated with control medium, TGF-β, or TGF-β plus eupatilin (50 μM). Anti-fibrogenic effects were observed by phase-contrast light microscopy. (c) A list of 35 CDs, grouped by chemical moieties coupled to the chromone scaffolds or the phenyl ring. Group A, including eupatilin, ONGA300 (jaceosidin), and ONGH300 (hispidulin), exerted potent anti-fibrogenic capacity. (d) Anti-fibrogenic effects of ONGH300, observed by phase-contrast light microscopy. (e) Anti-fibrogenic effects of ONGI200 (also called apigenin), observed by phase-contrast light microscopy.

residues (Fig. 1b). HSCs play dominant roles in the initiation and perpetuation of liver fibrosis [22]. Accordingly, to develop an efficient cell-based fibrosis assay, we established a mouse hepatic stellate cell (HSC) line called ONGHEPA1. These cells had a mesenchymal morphology, expressed GATA4 but not cytokeratin 18 (Fig. S2a and S2b), and displayed CD29, CD44, CD71, or CD106 on their surface (Fig. S2c), strongly indicating mesenchymal origin. Based on these features, we concluded that ONGHEPA1 is a mouse primary HSC line.

When ONGHEPA1 cells were stimulated with TGF-β, robust transdifferentiation into myofibroblasts occurred within 12 h. However, eupatilin completely inhibited the TGF-β–induced fibrosis at concentrations of 50 μM or above (Fig. S3a). Maximal induction of *Col11a1* and *Periostin* mRNAs, which are the signature genes of myofiboblasts, was determined by real-time PCR after 6 h and 9 h of TGF-β treatment, respectively (Fig. S3b). Pretreatment of ONGHEPA1 with eupatilin for 1–6 h did not diminish fibrosis, suggesting that TGFR-elicited signal transduction is necessary for the drug's ability to blunt fibrosis (Fig. S4).

Using this cell-based anti-fibrosis assay, we identified the carbon residues critical for anti-fibrotic potential of eupatilin, represented by colored font in Fig. 1: C2 (yellow), C3 (purple), C6 (red), and C7 (green). Next, we selected 35 CDs based on chemical similarities to eupatilin, classified them into five sub-groups, and evaluated their anti-fibrotic effects (Fig. 1c). The CDs belonging to Group A had significant anti-fibrotic activity: eupatilin itself; ONGE200, also known as hispidulin; and ONGA200, also known as jaceosidin. The latter two compounds are the most closely chemically related to eupatilin among the CDs tested. However, all of these compounds differ in terms of the chemical residues coupled to the phenyl ring. Eupatilin and ONGE200 had marked anti-fibrotic effects (Fig. 1b and Fig. S5a), whereas ONGA200 was weakly anti-fibrotic but cytotoxic at 50 μM (Fig. S5b), suggesting that the functional groups linked to the phenyl ring contribute to anti-fibrotic activity. ONGI300, in which two hydroxy groups are coupled to the phenyl ring, weakly inhibited fibrosis but promoted cell death, suggesting that chemical alteration of the phenyl ring also affects anti-fibrotic activity (Fig. S5c).

To explore the importance of the eight carbons of the CS in terms of structure–function relationship, we focused on two anti-fibrotic CDs (eupatilin and ONGE200) alongside the remaining 33 CDs. When a methoxy residue was coupled to C3, as in ONGH300, the anti-fibrotic effect was eliminated, and the compound was toxic (Fig. 1d). In comparison with ONGE200, ONGI200 (apigenin) lacks only the methoxy group coupled to C6. ONGI200 had no anti-fibrotic effect, suggesting that C6 is an important constituent of the CS, and that methoxylation of this position is necessary for prevention of fibrosis (Fig. 1e). We also noticed that ONGC200, in which the hydroxy residue at C7 of ONGE200 is replaced with a methoxy group, completely lost the anti-fibrotic effect, suggesting that C7 is also a critical component of the CS (Fig. S6a). In addition, methoxylation at C2 of ONGA300, yielding a compound equivalent to ONGH300, abolished its anti-fibrotic capacity, suggesting that the presence of a bulky group at C2 may affect anti-fibrotic potential (Fig. S6b). The same held true for ONGD400, a highly cytotoxic stereoisomer of ONGH300 in which C3 is methoxylated (Fig. S6c). Taken together, our data confirm that chemical modifications on the CS are only tolerated at specific carbons, indicating that the anti-fibrotic effects of these compounds obey a stringent structure–activity relationship.

3.2. Eupatilin exerts potent anti-fibrotic activity by acting directly on myofibroblasts

Several residential cell niches, including fibroblasts, myofibroblasts, pericytes, and bone marrow–derived fibrocytes may contribute to generation of pathogenic myofibroblasts *via* EMT [23,24]. A unified theory on generation of myofibroblasts remains elusive in the pulmonary fibrosis [25,26]. To date, however, the fibrotic effect of TGF-β on human lung epithelial cells (HLECs) has not been explored. In contrast to the situation for liver fibrosis, the major cell type that differentiates into

pathogenic myofibroblasts in the lung remains to be elucidated. To address this issue, we first sought to identify CDs that effectively inhibited TGF-β–mediated fibrosis. To this end, we assessed the effects of these compounds, particularly eupatilin, on induction of the *in vitro* transdifferentiation of human lung fibroblasts derived from IPF patients (diseased human lung fibroblasts: DHLFs) to myofibroblasts [27]. Relative to TGF-β alone, stimulation of DHLFs with TGF-β plus eupatilin resulted in significant growth arrest, whereas, when cells were stimulated with TGF-β plus pirfenidone, no growth arrest was observed after 48 or 72 h (Fig. 2a). However, cell proliferation assays revealed that eupatilin and pirfenidone both substantially attenuated proliferation of DHLFs during the first 12 h of treatment. Consistent with this, we observed that eupatilin inhibited cell proliferation somewhat more effectively than pirfenidone (Fig. 2b). Immunochemistry revealed that eupatilin completely inhibited α–smooth muscle actin (αSMA) expression, being a hallmark of myobibroblasts, whereas pirfenidone had no effect (Fig. 2c). Non-treated DHLFs expressed low levels of αSMA, suggesting that a fraction of myofibroblasts may already exist in the lung niches of IPF patients. Likewise, expression of a major EMT-inducible gene, *POSTN* (periostin), was inhibited by eupatilin not but pirfenidone (Fig. 2d). Periostin, an important regulator of ECM biogenesis, also serves as a ligand for integrin αvβ3 [28]. As with TGF-β, platelet-derived growth factor receptor (PDGFR) signaling has also been implicated in fibrosis [29]. However, PDGF was incapable of driving differentiation of ONGHEPA1 cells in the presence of eupatilin (Fig. S7a and S7b). Taken together, these findings indicate that eupatilin acts directly on pathogenic myofibroblasts, disarming the cells, *via* a MOA distinct from that of pirfenidone.

EMT plays a central role in regulating the morphological transition of epithelial cells into mesenchymal cells during both tumor metastasis and embryogenesis [30]. To determine whether eupatilin affects the EMT of HLECs in this manner upon stimulation with TGF-β, we measured the expression of representative EMT genes *via* real-time PCR. Surprisingly, none of the genes we examined, including *SNAI1* (Snail1), *SNAI2* (Snail2), *ZEB1*, *ZEB2*, *VIM* (vimentin), and *CDH1* (E-cadherin), were induced in HLECs in response to TGF-β (Fig. S8), suggesting that HLECs play no or little role in TGF-β–induced generation of myofibroblasts in the lung niche. Similarly, we detected no induction of *POSTN* (periostin), *COL1A1* (Collagen1α1), and *COL11A1* (Collagen11α1) (data not shown). Interestingly, eupatilin significantly induced *SNAI1*, *SNAI2*, and *ZEB2* in HLECs, whereas pirfenidone did not affect expression of these genes. We cannot explain this unanticipated observation.

To validate the results of our real-time PCR experiments, we used A549 cells, a human lung adenocarcinoma cell line of alveolar basal epithelial cell origin that has been widely used for analyses of tumor metastasis and EMT induction [31]. TGF-β rendered A549 cells somewhat blastogenic, and their cell morphology was altered: the treated cells became round, suggesting that eupatilin can reorganize cytoskeletal structures (Fig. S9a). *SNAI1* and *VIM* were significantly upregulated by TGF-β, but these effects were dramatically attenuated by eupatilin (Fig. S9b).

Taken together, these data suggest that eupatilin inhibits proliferation and drives morphological change in DHLFs by negatively regulating the transdifferentiation into myofibroblasts. In previous work, we demonstrated that eupatilin does not promote cell death [18]. Unexpectedly, our findings indicated that the HLEC/TGF-β axis does not contribute to IPF.

3.3. Actin depolymerization by eupatilin disarms formation of latent TGF-β complex, preventing TGF-β receptor signaling

Myofibroblasts play pivotal roles in tissue scarring, but the molecular and cellular mechanisms associated with the therapeutic efficacy of

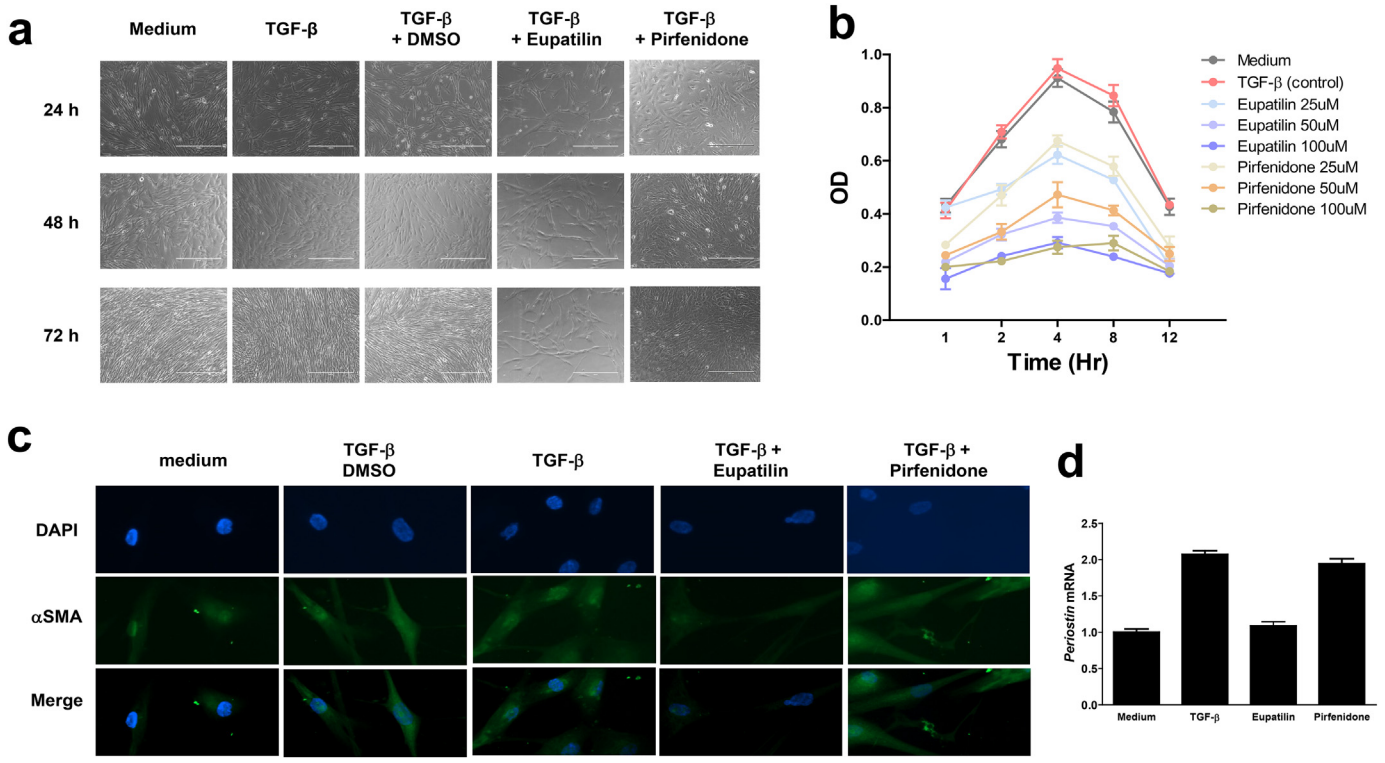

Fig. 2. Inhibition of TGF-β–induced fibrosis by eupatilin. (a) DHLFs (5×10^6 cells) were seeded in fibroblast growth medium (FBM), grown overnight, and then stimulated with control medium, TGF-β (5 ng/ml), TGF-β plus eupatilin (50 μM), or TGF-β plus pirfenidone (50 μM) for 72 h. Morphological change was monitored by phase-contrast microscopy at 40× magnification. (b) Proliferation of DHLFs was substantially attenuated by eupatilin and pirfenidone. DHLFs were treated with 0, 25, 50, and 100 μM eupatilin or pirfenidone in the presence of TGF-β for the indicated periods prior to estimation of cell proliferation using the CCK-8 assay. The experiment was performed in triplicate. (c) Eupatilin, but not pirfenidone, inhibited TGF-β–induced α–smooth muscle actin (αSMA). ICC was performed using anti-mouse αSMA antibody. (d) Total RNA was isolated from DHLFs stimulated with control medium, TGF-β, TGF-β plus eupatilin, or TGF-β plus pirfenidone for 48 h, and then subjected to real-time PCR analysis using primers against *POSTN* or *VIM*. Standard deviations were calculated from the results of three independent PCRs.

anti-IPF drugs have yet to be elucidated. Nintedanib is known to be an angiokinase inhibitor that antagonizes TGF-βR, FGFR, and PDGFR, whereas the mode of action (MOA) of pirfenidone remains elusive [32]. To investigate the MOA(s) of eupatilin, we used ONGHEPA1 cells, an established mouse HSC cell line. As shown in Fig. 3a, TGF-β induced αSMA expression, concomitant with a change in cell morphology; these effects were completely inhibited by eupatilin, as was the inhibition of *Col11a1*. We then compared the anti-fibrotic effects of pirfenidone, nintedanib, and apigenin (ONGI200), a CS-containing synthetic compound, with the activity of eupatilin. Nintedanib and eupatilin completely inhibited fibrosis, but the resultant cell shapes were distinct (Fig. 3b), suggesting that the two drugs mitigated TGFR signaling *via* different mechanisms, and that the MOA of pirfenidone is not directly related to TGFR signaling. Activation of Erk [33] or Smad3 [34] is required for TGF-β–mediated induction of the *in vivo* fibrogenesis. Eupatilin did not alter phosphorylation of Erk, Smad2, or Akt, but it significantly inhibited phosphorylation of Smad3 within 1 h after TGF-β treatment (Fig. 3c).

Formation of latent TGF-β complex loaded with processed active TGF-β, along with LTBP1 or LTBP4, integrin αvβ3 (or other integrin β family member), and LAP1, in the ECM is prerequisite for activation of TGFR [35]. Integrin αvβ3 is anchored to actin filaments at focal adhesions [36], and we showed previously that eupatilin has potent actin depolymerizing activity [18]. To explore the anti-fibrotic potential of eupatilin, we conducted a series of ICC experiments involving inhibition of actin depolymerization, which results in dismantling of the latent TGF-β complex. As shown in Fig. 3d, actin stress fibers were formed *via* stimulation of ONGHEPA1 with TGF-β, and only eupatilin was able to depolymerize actin. Neither pirfenidone nor nintedanib was capable of dismantling actin fibers. More importantly, a central cargo protein, LTBP1, was readily detected in the ECM and completely disappeared from the ECM, strongly suggesting that actin depolymerization induced by eupatilin plays a central role in the destruction of latent TGF-β complex, thereby mitigating TGFR signaling. Interestingly, pirfenidone did not affect the level of LTBP1 in the ECM, whereas nintedanib significantly inhibited LTBP1 expression, suggesting that LTBP1 in the ECM is a target of nintedanib. Latency-associated peptide 1 (LAP1) was constitutively expressed in both cytoplasm and ECM, but none of the tested drugs attenuated its expression at the mRNA level. By contrast, LTBP4 and integrin αvβ3 were induced by TGF-β, but were retained in the cells (Fig. S10). Moreover, none of the drugs affected the ECM expression of LTBP4 or integrin αvβ3. These data indicate that one major MOA of eupatilin is actin depolymerization, which leads to dismantling of the latent TGF-β complex.

3.4. Eupatilin is a potent inducer of dedifferentiation

In the work described thus far, ONGHEPA1 cells were simultaneously stimulated with TGF-β or PDGF in the presence of eupatilin. In subsequent experiments, we extensively investigated anti-fibrotic capacity using a sequential stimulation paradigm in which ONGHEPA1 cells were first stimulated with TGF-β or PDGF for 24 h, washed, and then re-stimulated with TGF-β plus a CD (eupatilin or ONGE200; both are anti-fibrotic) for another 24 h. Their morphological changes were monitored by phase-contrast microscopy, as shown in Fig. 4a and c. These data clearly demonstrate that both eupatilin and ONGE200 are capable of preventing fibrosis, and indeed likely reversed the fibrosis that already existed. Real-time PCR revealed downregulation of two EMT-inducible genes, *POSTN* and *FN1* (fibronectin 1), mirroring the anti-fibrotic activities (Fig. 4b and d). Notably in this regard, previous work

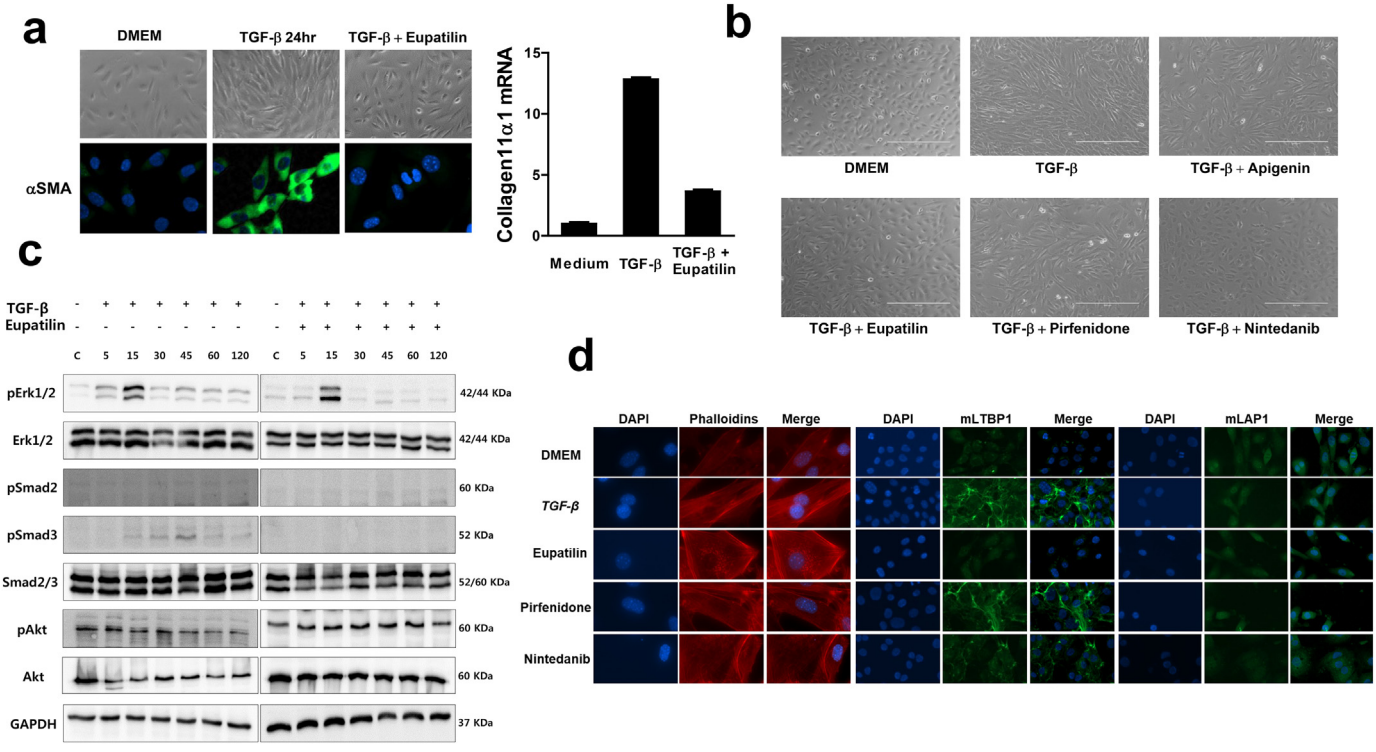

Fig. 3. Eupatilin inhibits TGF-β–mediated cellular response by dismantling latent TGF-β complex, depolymerizing actin, and modulating Smad3. (a) ONGHEPA1 cells were stimulated with TGF-β (5 ng/ml) or TGF-β plus eupatilin (50 μM) for 24 h, and morphological changes were monitored under a light microscope. ICC was performed using anti-mouse αSMA antibody. Total RNAs were isolated from ONGHEPA1 cells stimulated with medium, TGF-β, or TGF-β plus eupatilin for 48 h, and then subjected to real-time PCR analysis using primers against *Col11a1*. (b) ONGHEPA1 cells were grown and stimulated with medium, apigenin, eupatilin, pirfenidone, or nintedanib in the presence or absence of TGF-β for 24 h, and then anti-fibrogenic activity was monitored. (c) Kinetics of eupatilin-induced Erk, Smad2, Smad3, and Akt phosphorylation in the presence of TGF-β. Western blot analyses of pErk1/2, pSmad2, pSmad3, and pAkt levels were performed in whole-cell lysates (30 μg) of ONGHEPA1 cells incubated with TGF-β or TGF-β and eupatilin for 0, 5, 15, 30, 45, 60, and 120 min. (d) Actin depolymerization and latent TGF-β complex–associated protein expression in eupatilin, pirfenidone, and nintedanib-treated ONGHEPA1 cells in the presence of TGF-β. ONGHEPA1 cells stained for F-actin (phalloidin, red), mLTBP (green), mLAP1 (green), and DAPI (nuclei, blue). Only eupatilin was able to depolymerize actin.

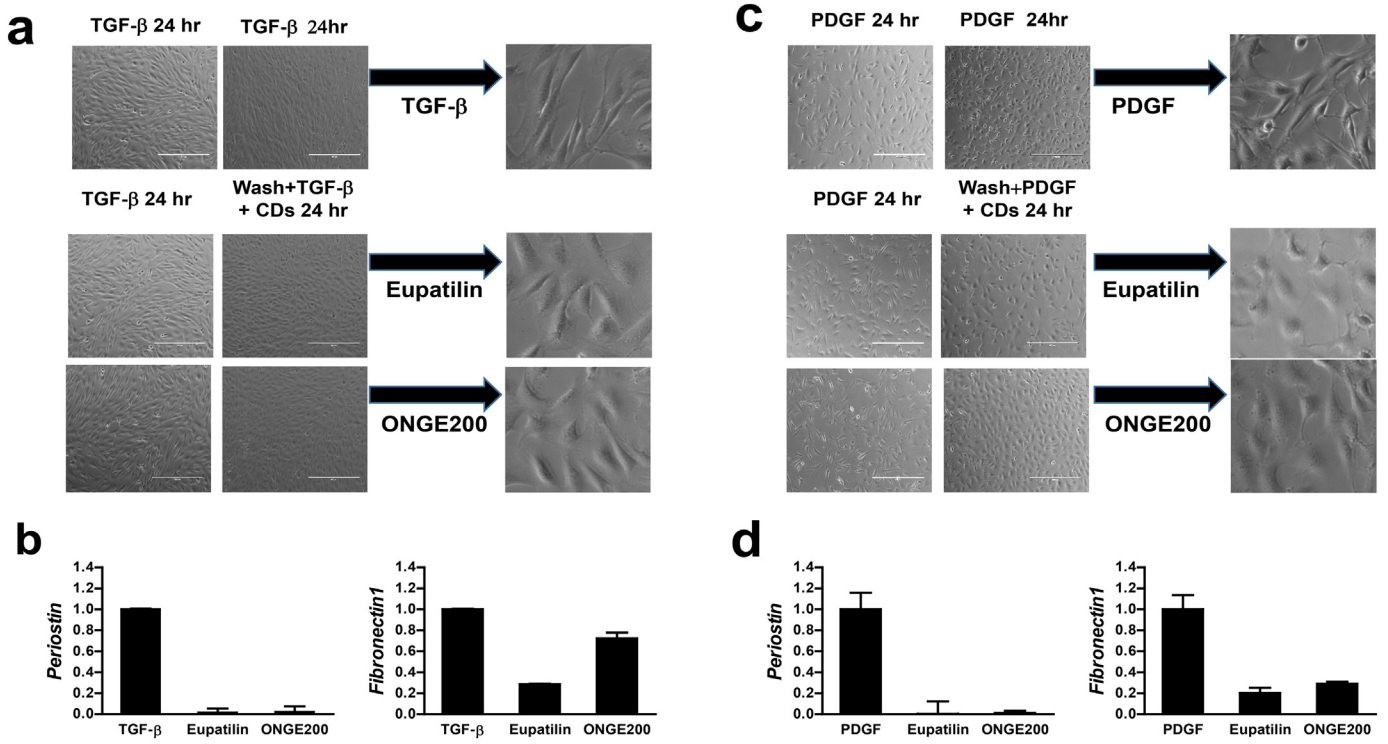

Fig. 4. Dedifferentiation is associated with eupatilin-mediated anti-fibrotic capacity. (a and c) ONGHEPA1 cells were stimulated with TGF-β or PDGF for 48 h, and another set of ONGHEPA1 cells was first stimulated with TGF-β or PDGF for 24 h until myofibroblasts were predominant, and then further stimulated with both TGF-β + eupatilin or TGF-β + ONGE200 and PDGF + eupatilin or PDGF + ONGE200. Morphological changes were monitored under a light microscope. (b and d) Total RNA was isolated from ONGHEPA1 cells stimulated as described above and subjected to real-time PCR analysis using primers against *Postn* or *Fn1*. Standard deviations were calculated from the results of three independent PCRs.

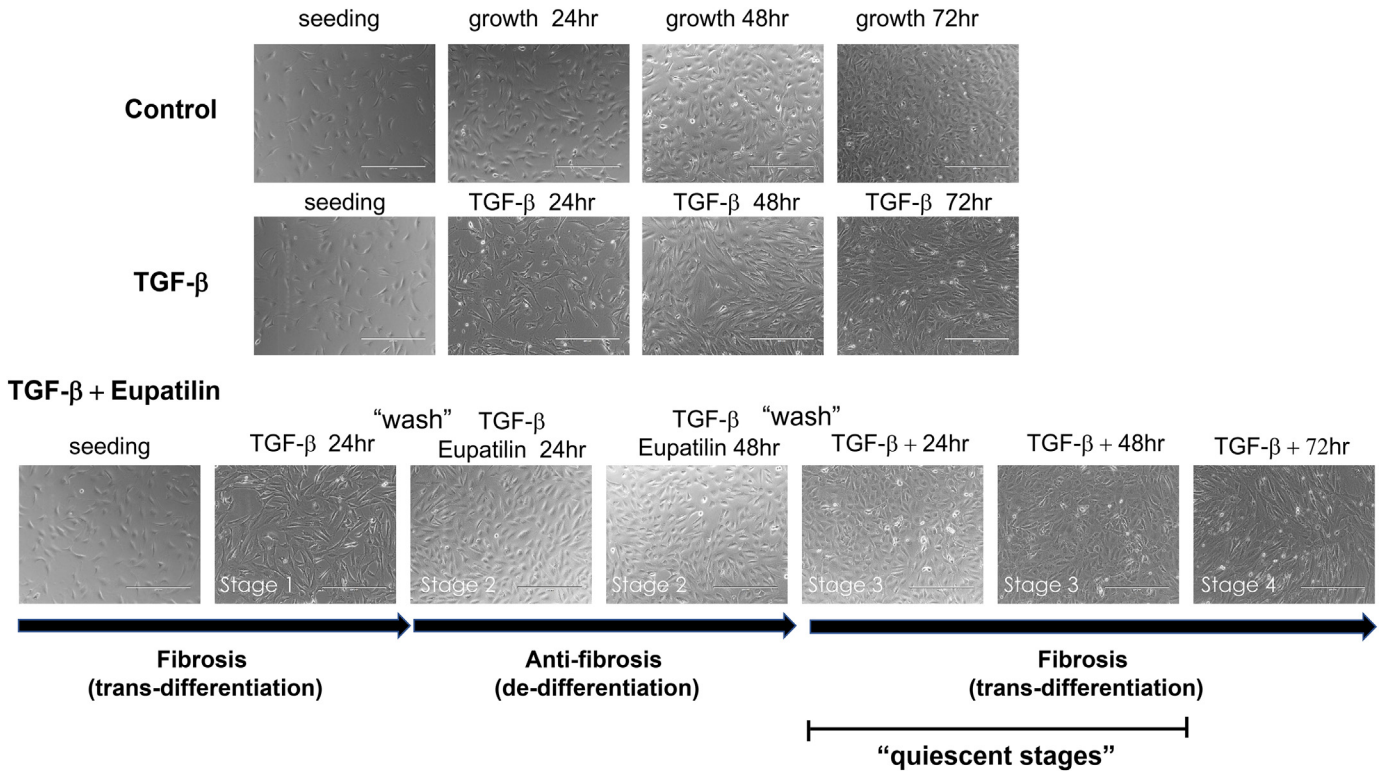

Fig. 5. Dedifferentiation occurs during blocking of fibrosis by eupatilin. ONGHEPA1 cells were stimulated with TGF-β for 72 h or not stimulated; in parallel, another set of ONGHEPA1 cells were stimulated with TGF-β for 24 h, washed, and stimulated with TGF-β + eupatilin for 48 h. After washing, the resultant cells were continuously stimulated with TGF-β for 72 h. Morphological changes were monitored under a light microscope. Each pathological stage is indicated by arrows and corresponding terms.

has shown that pathogenic myofibroblasts may become non-fibrotic intermediate cell types *via* reversal or induction of quiescence during recovery from human liver fibrosis [37].

To recapitulate this *in vivo* observation, we set up an *in vitro transdifferentiation and dedifferentiation* experiment in which transdifferentiation (fibrosis) was followed by dedifferentiation (anti-fibrosis). In these experiments, TGF-β–treated or non-treated ONGHEPA1 cells were grown for 72 h; in parallel, another set of ONGHEPA1 cells was stimulated with TGF-β for 24 h (during which all cells became myofibroblasts), washed with PBS buffer, and re-stimulated with TGF-β plus eupatilin for another 48 h. Surprisingly, all cells became non-myofibrogenic, more likely being the parental ONGHEPA1-like cells (Fig. 5). After the resultant cells were washed and replated, we stimulated them with TGF-β alone for an additional 72 h. We found that 48 h was the minimum time required for trans-differentiation into myofibroblasts. This period represents a quiescent stage after which the cells differentiated into myofibroblasts, suggesting that the cell-based *in vitro* fibrosis assay may be complementary to what has been observed during recuperation from liver fibrosis *in vivo*.

Taken together, these observations demonstrate that eupatilin is a potent anti-fibrotic drug that may be able to dedifferentiate pathogenic myofibroblasts into quiescent intermediate cell types. This finding, in conjunction with our observation of actin depolymerization by eupatilin, prompted us to investigate whether eupatilin could exert a therapeutic effect on lung fibrosis.

3.5. Eupatilin significantly improves the onset of BLM-induced lung fibrosis

To establish the BLM mouse model, eupatilin or pirfenidone at 100 mg/kg (mpk) was administered orally, twice per day, followed by one intratracheal administration of bleomycin; daily oral drug intake continued for the next 14 days (Fig. 6). At 100 mpk, the molar concentration of pirfenidone is 2-fold higher than that of eupatilin. Oral administration of pirfenidone over 100 mpk resulted in hepatotoxicity, so we selected 100 mpk to compare the therapeutic efficacies of the two drugs. We observed significant reductions in the levels of soluble collagen and hydroxyproline (HP), as well as changes in collagen histomorphometry, in the drug-treated animals (Fig. 6a–c, see Appendix for raw data with statistical analysis). Interestingly, TGF-β production level was highest in the pirfenidone-treated mice (Fig. 6d), suggesting that the putative MOA of pirfenidone involves downregulation of *in vivo* TGF-β production, presumably by immune cells [38].

Fibrotic tissues are characterized by notable collagen deposition, along with proliferation of myofibroblasts or infiltration by inflammatory cells [39]. We performed hematoxylin/eosin (H&E) staining to visibly stain proliferative and infiltrated cells, and used Sirius Red to stain regions of collagen deposition. As seen in Fig. 6e, BLM-treated lungs harbored the largest number of H&*E*- and Sirius Red–stained cells, and pirfenidone treatment weakened the intensities of both stains. More intriguingly, eupatilin-treated lungs contained the smallest number of proliferative cells and very pale collagen staining, suggesting that eupatilin has more potent cell regeneration potential than pirfenidone.

Next, to confirm the anti-fibrotic potential of eupatilin, we examined the dose-dependence of its effects. At doses of 100 and 200 mpk, but not a lower dose of 50 mpk, we observed a statistically significant increase in the levels of soluble collagen and hydroxyproline. Overall, pirfenidone (100 mpk) had less of an inhibitory effect on collagen histomorphometry and hydroxyproline than eupatilin (200 mpk), and this difference was statistically significant (Fig. 6f and g, see Appendix for raw data with statistical analysis). It should be noted that the molar concentrations of eupatilin (200 mpk) and pirfenidone (100 mpk) are equal, suggesting that eupatilin is a more potent anti-fibrotic agent. As above, pirfenidone (100 mpk) was associated with less TGF-β production than eupatilin (200 mpk) (Fig. 6h), again suggesting that the MOA of pirfenidone involves decreasing the production of TGF-β in the lung. Nevertheless, eupatilin (100 or 200 mpk) was also able to significantly inhibit TGF-β production. Tissue regenerative capabilities were greater under both doses of eupatilin than under pirfenidone because magnitude of inflammatory foci indicated by yellow arrows or degree of collagen deposit denoted by arrow heads (Fig. 6i).

Eupatilin is efficiently absorbed into the upper GI tract, appears in plasma within 1 h of ingestion, and is also readily detected in lung tissue lysates [40]. Eupatilin glucuronide was the major metabolite in plasma (Fig. S11a), whereas free eupatilin predominated in lung, liver, and kidney tissues within 2 h of ingestion (Fig. S11b–d). No eupatilin glucuronide was detected by NMR in these tissues. By contrast, parental pirfenidone was present in large concentrations in plasma and all three tissues. These observations suggest that orally administered eupatilin is rapidly disseminated to these tissues upon deglucuronidation presumably occurring in the liver followed by deconjugation of the glucuronide moiety in these tissues. Lung tissues express high levels of deconjugating enzymes [41]. Eupatilin was present in the lung exclusively as the free form, but at concentrations at least 100-fold lower than those of pirfenidone, suggesting that it is extremely potent against lung fibrosis.

Pirfenidone is hepatotoxic at high concentrations over 100 mpk [42], whereas the toxicity of eupatilin remains unknown. To explore this issue, we performed a full set of liver function tests using mouse plasma. As shown in Fig. S12, we detected no hepatotoxicity in mice treated with either pirfenidone (100 mpk) or eupatilin (200 mpk), suggesting that eupatilin does not elicit hepatotoxicity.

To investigate whether eupatilin has anti-fibrotic efficacy in the context of lung fibrosis, we used a therapeutic BLM model, as schematized in Fig. 7a. Collagen histomorphometry, soluble collagen production, and TGF-β production were measured in lung lysates. We observed equivalent significant reductions in collagen morphometry under eupatilin (100 and 200 mpk) and pirfenidone (100 mpk) (Fig. 7b, see Appendix for raw data with statistical analysis). Significant reductions in soluble collagen were observed under pirfenidone (100 mpk) and eupatilin (200 mpk), but not eupatilin (100 mpk) (Fig. 7c). Consistent with our prior results, pirfenidone (100 mpk) inhibited TGF-β production to a somewhat greater extent than eupatilin (200 mpk) (Fig. 7d); by contrast, eupatilin (100 mpk) did not reach a statistically significant effect. Histological staining revealed that eupatilin induced somewhat more cell regeneration than pirfenidone, as indicated by the absence of inflammatory foci and collagenous deposits in eupatilin-treated samples (denoted by yellow arrows and yellow arrowheads, respectively) (Fig. 7e).

3.6. Inhibition of transdifferentiation into myofibroblasts by eupatilin may be responsible for its anti-fibrotic activity

We next asked how eupatilin blocks the TGF-β–induced myofibroblast transdifferentiation. To this end, we stimulated ONGHEPA1 cells with TGF-β or TGF-β plus eupatilin, and then conducted global gene expression analyses by RNA-seq. Using a bioinformatics approach, we constructed an unbiased interactome that contained several notable hubs, including the collagen gene family (*Col11a1*) and the genes encoding components of the cytoskeleton (*Actinin*, α *smooth muscle aorta*, *Troponin 1* and *2*, *Tropomyosin 2*, *Myosin-heavy chain 1* and *Myosin-light chain 9*, and *Laminin 4*) (Fig. 8). Notably, *integrin α1 β3* played pivotal roles in connecting these hubs. Expression of *Slug* (also called *Snail2*), a major transcription factor deeply involved in the EMT, was regulated by eupatilin. Two cell-cycle hubs, encoded by *Cdk4* and *Fos*, seemed to be pronouncing, potentially explaining the eupatilin-induced growth arrest in DHLFs. Several genes encoding receptors, including members of the semaphorin receptor family, a cholesterol receptor (*Vldr*), and *CD44*, formed significant hubs. One notable signaling molecule associated with eupatilin-mediated-inhibition of myofibroblast transdifferentiation was adenylate cyclase 9 (encoded by *Adcy9*), which is involved in small G-protein activation. This feature should be investigated further in future studies.

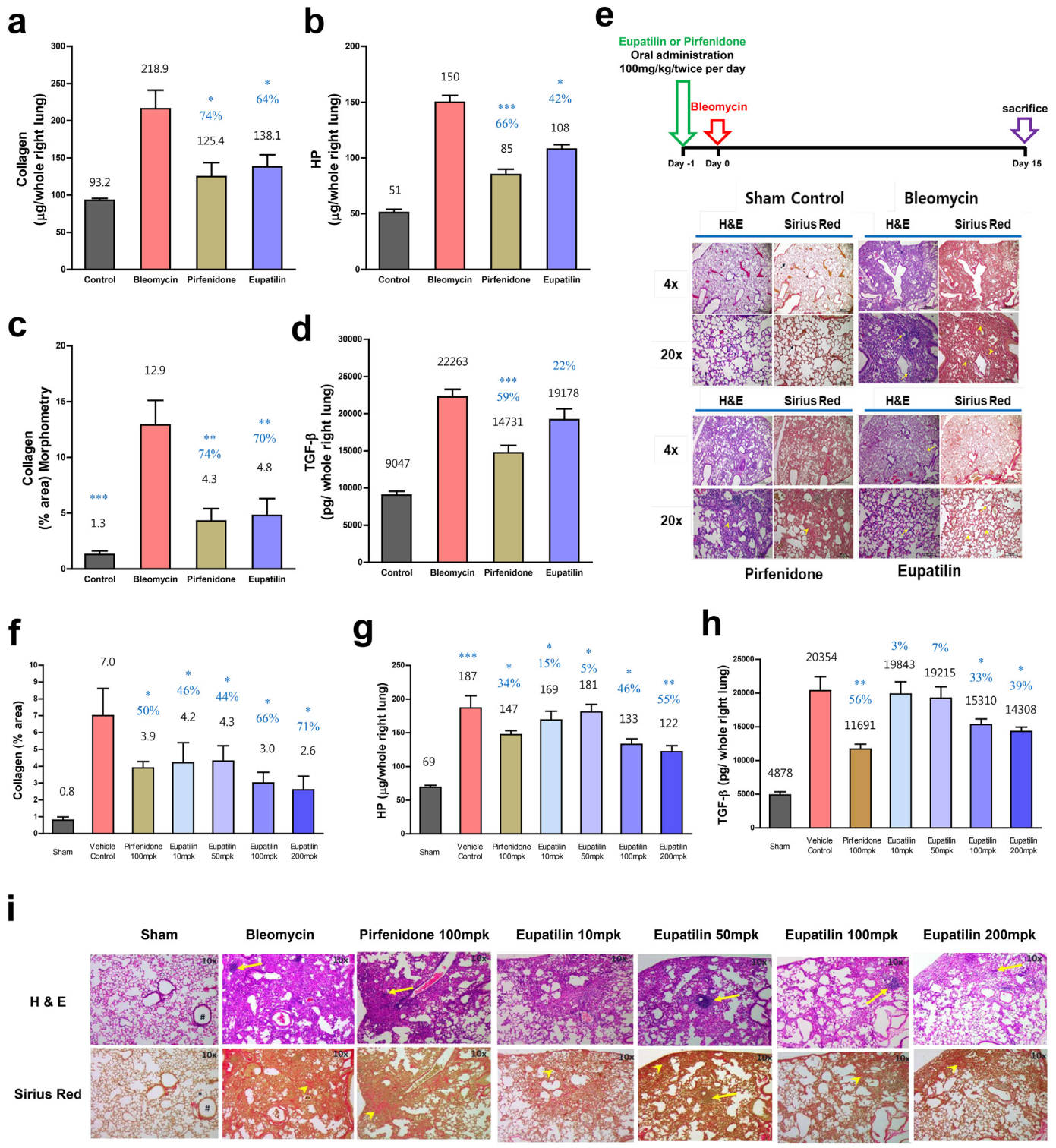

Fig. 6. Prevention of BLM-induced lung fibrosis by eupatilin. One intratracheal injection of BLM gave rise to fulminant fibrosis of the lungs in all mice. Vehicle, pirfenidone (100 mpk), or eupatilin (100 mpk) was orally administered twice per day for 14 days, and then lung tissue lysates and plasma were prepared. (a) Soluble collagen from whole right lung was measured. * indicates statistical significance ($p < 0.05$, Student's *t*-test). (b) Levels of hydroxyproline (HP) were measured and subjected to *t*-test. **, $p < 0.05$ *via* *t*-test. (c) Collagen histomorphometry was examined and compared. Statistical significance was calculated by Student's *t*-test. **, $p < 0.01$; ***, $p < 0.001$. (d) TGF-β in whole right lung was measured by ELISA. (e) Paraffin sections of lung tissues were stained with H&E or Sirius Red and examined by phase-contrast microscopy at 4× or 20× magnification. Infiltrating cells and collagen deposition were detected. (f) Vehicle (0.5% CMC + 1% Tween 80), pirfenidone (100 mpk), or various concentrations of eupatilin (10, 50, 100, or 200 mpk) were orally administered to C57BL/6 J mice 1 day before administration of bleomycin. BLM was intratracheally injected, and the drugs were administered orally twice per day for 14 days, after which lung tissues and plasma were collected, and histomorphometry was performed. Statistical significance was calculated by Student's *t*-test (*, $p < 0.05$; **, $p < 0.01$). (g) Levels of hydroxyproline (HP) were measured and subjected to Student's *t*-test as described above. ***, $p < 0.001$. (h) Whole right lung tissue lysates were subjected to ELISA for mouse TGF-β. (i) Paraffin sections of lung tissues were stained with H&E and Sirius Red, and then observed by phase-contrast microscopy (10× magnification). Inflammatory foci and collagen deposits are denoted by yellow arrows and yellow arrowheads, respectively.

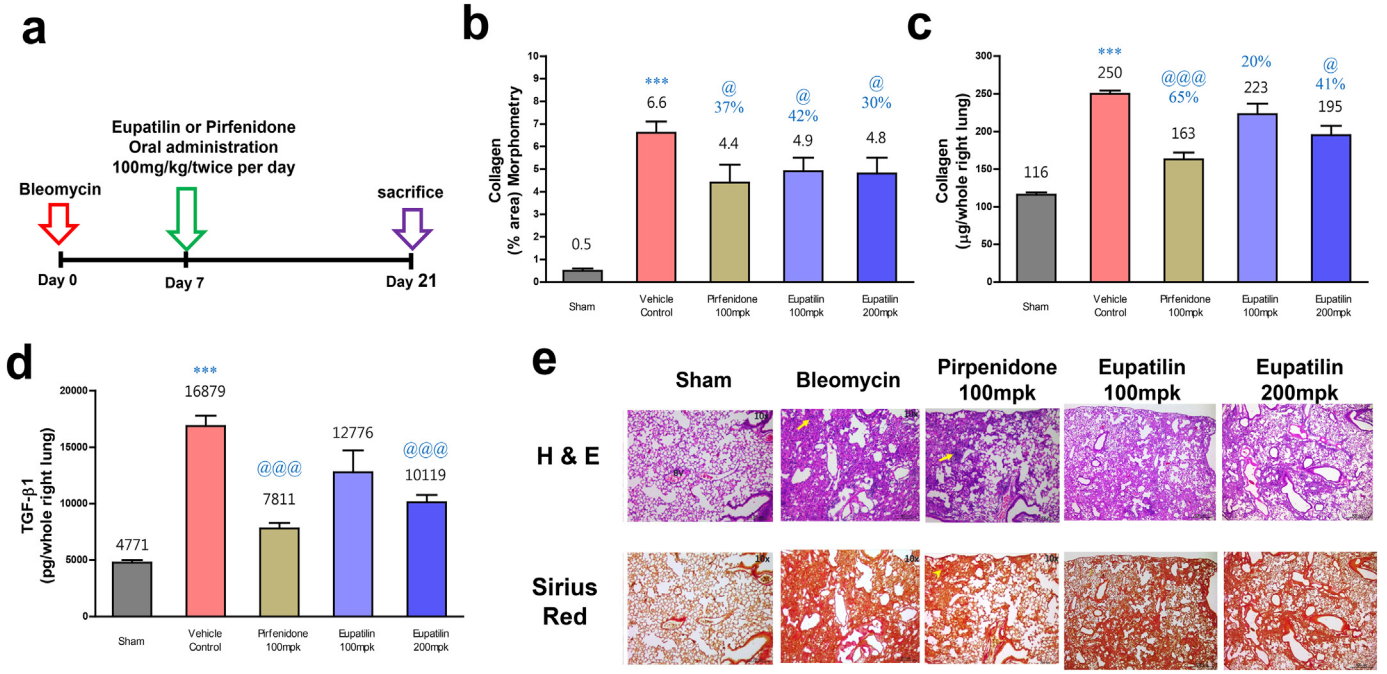

Fig. 7. Treatment of BLM-induced lung fibrosis with eupatilin. (a) Bleomycin was intratracheally administered into mice at day 0, and lung fibrosis was allowed to develop for 7 days. Eupatilin (100 or 200 mpk) or pirfenidone (100 mpk) was orally administered for 14 days. Lung lysates and tissue paraffin sections were prepared. (b) Histomorphometry was examined, and statistical significance was calculated by Student's *t*-test; *, $p < 0.05$. (c) Soluble collagen from whole right lung was measured. *, $p < 0.05$ (Student's *t*-test). (d) TGF-β in whole right lung was measured by ELISA. ***, $p < 0.001$ (Student's *t*-test). (e) Paraffin sections of lung tissues were stained with H&E or Sirius Red and examined by phase-contrast microscopy at 4× or 20× magnification. Inflammatory foci and collagen deposits are denoted by yellow arrows and yellow arrowheads, respectively.

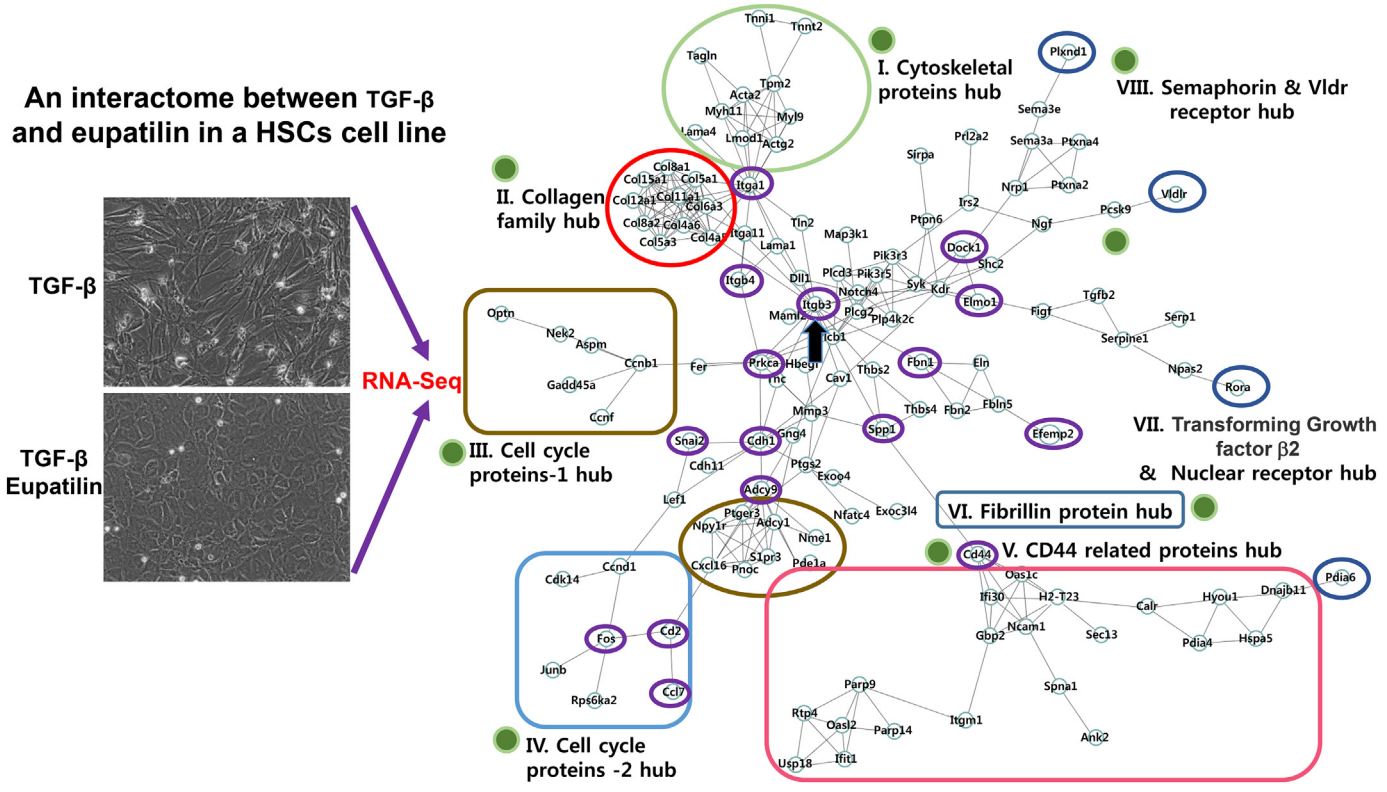

Fig. 8. The interactome generated by simultaneous stimulation of ONGHEPA1 cells with TGF-β and eupatilin reveals a transdifferentiation and/or dedifferentiation pathway. Total RNA was isolated from ONGHEPA1 cells treated with TGF-β or TGF-β plus eupatilin. One microgram of RNA from each sample was subjected to RNA-seq, yielding 60 Gb of sequence, and gene interactions were established as described in Materials and Methods. Threshold for selection of a gene as differentially regulated was $p < .05$. Eight hubs are represented by colored boxes or ovals, and critical nodes are depicted as purple ovals.

To identify the most critical genes involved in the inhibition of myofibroblast transdifferentiation by eupatilin, we identified a set of 103 genes that were maximally induced by TGF-β and maximally repressed by eupatilin (data not shown). The vast majority of these genes encode factors involved in promoting the EMT: cell adhesion molecules, several enzymes involved in oxidation or reduction of procollagen, metalloproteases, proteoglycans, and TGFR signaling factors. For instance, follistatin-like 1 (Fstl1) plays a pivotal role in pulmonary fibrosis [43], and deficiency of *Fstl1* completely protects mice from bleomycin-induced lung fibrosis; consistent with this, *Fstl1* was downregulated by eupatilin. In addition to gene expression analysis, we performed proteomic analysis to determine which of the proteins encoded by the 103 eupatilin-repressed genes were actually downregulated in ONGHEPA1 cells treated with TGF-β plus eupatilin (Fig. S13). LC-MS/MS analysis of ONGHEPA1 cells stimulated with TGF-β or TGF-β plus eupatilin identified 2545 proteins. The relative abundances of the identified proteins under the two conditions were calculated based on the normalized spectral abundance factor (NSAF), a method for spectral counting. Of the 2545 proteins detected, 398 exhibited statistically significant changes (p-value <.05, Student's t-test), and 196 of those were downregulated >1.5-fold in ONGHEPA1 cells stimulated with TGF-β plus eupatilin. Comparison of these 196 proteins with the 103 genes repressed by eupatilin yielded 11 matches: *Caprin1*, *Col1a1*, *Cola3a1*, *Dpsyl3*, *Ehd2*, *Fn1*, *Hspg2*, *Map4*, *P4ha1*, *Plod2*, and *Slt3* (Fig. S13). In Gene Ontology analysis of these 11 proteins, the most enriched biological process was ECM organization, and most of these genes are involved in EMT-related processes, *e.g.*, cellular migration (*Slit3*, which encodes Slit Homolog 3) [44], remodeling of the cytoskeleton (*Plod2*, encoding procollagen-lysine,2-oxoglutarate 5-sioxygenase 2) [45], and cell-cycle arrest (*Caprin1*, which encodes cell cycle–associated protein 1) [46]. Although the functions of these proteins need to be further verified, it is reasonable to assume that downregulation of these proteins in ONGHEPA1 cells stimulated with TGF-β plus eupatilin was closely associated with inhibition of myofibroblast differentiation or proliferation. These eupatilin-repressible genes represent new molecular targets for anti-fibrotic therapies.

4. Discussion

Fibrosis refers to a disease state with multifactorial causes that leads to tissue scarring [2]. Although the initial phase of fibrosis seems to involve inflammation, the overall progression is only partially explained by immunological dysfunction. Differentiation of epithelial cells, pericytes, bone-marrow-derived fibrocytes, diversified mesenchymal cells, or resident fibroblasts or even myofbroblasts into pathogenic myofibroblasts is a major mechanism underlying perpetuation of fibrosis [47], and the EMT provides the basis for this transdifferentiation. In the case of liver fibrosis, HSCs are the major cell type responsible for generation of myofibroblasts, but no analogous cell niches have been revealed for IPF, and our investigation of HLECs indicated that the EMT does not play a pivotal role in generation of myofibroblasts in the lung. It is of paramount importance to identify the cell niches associated with IPF [48]. >10 anti-IPF drug candidates have been rejected due to their unsatisfactory therapeutic efficacies [49]. The recent failure of a human anti–lysyl oxidase antibody to successfully treat IPF suggests that simple inactivation of collagen cross-linking enzymes may not be sufficient [50], and that knockdown of other extracellular or membrane-bound enzymes involved in ECM biogenesis is necessary to improve therapeutic efficacy. The results of combinatorial therapy with pirfenidone and nintedanib revealed that a simple combination of drugs does not always result in an additive or a synergistic effect [51]. Furthermore, neither drug is able to extend survival of IPF patients aged 65 years or more [52–54]. Our BLM experiments clearly showed that pirfenidone (100 mpk) could consistently suppress *in vivo* production of TGF-β. Similarly, eupatilin (200 mpk), representing a molar concentration equivalent to pirfenidone (100 mpk), significantly inhibited *in vivo* production of TGF-β as well. However, it remains unclear which lung residential cell types are primarily responsible for eliciting the generation of myofibroblasts that contribute to IPF. Based on our *in vitro* fibrosis assays, pirfenidone does not directly act upon myofibroblasts, whereas eupatilin is able to directly stimulate actin depolymerization, thereby dismantling latent TGF-β complex and disarming LTBP1. According to our RNA-seq analysis, *LTBP1* was more repressed by eupatilin than *LTBP2* and *LTBP4*, but neither pirfenidone nor nintedanib decreased the level of LTBP1 in the ECM. Moreover, integrin αvβ3 was expressed intracellularly but was not trafficked into ECM. At present, due to our inability to obtain specific antibodies, we do not know whether integrin αvβ6 is expressed at the protein level in ONGHEPA1 cells, an issue that must be addressed in future studies. The actin depolymerization activity of nintedanib was marginal at best, but like eupatilin, nintedanib acted directly on myofibroblasts, as demonstrated by both the HSC differentiation and ICC experiments. The results obtained with our cell-based fibrosis assay data strongly suggest that nintedanib is significantly cytotoxic, and that the resultant cell shape is distinct from that of eupatilin-treated cells.

A comparison of *in vivo* cell regeneration capacity between eupatilin and pirfenidone using tissue staining revealed that the former was superior in terms of the degree of cell infiltration or proliferation and the deposition of soluble collagen, suggesting that eupatilin represents a strong candidate for ameliorating IPF. Notably in this regard, eupatilin was able to reverse fibrosis at the levels of morphology and global gene expression. This sort of explicit dedifferentiation of myofibroblasts into a quiescent state, which can also be trans-differentiated into myofibroblasts by TGF-β, has not been previously described. However, intermediate quiescent cells are frequently observed during recovery from human liver fibrosis [55–59]. In the case of sequential stimulation, although reversion to a normal ONGHEPA1-like morphology was evident, 81% of the genes that were differentially regulated in cells treated with TGF-β and TGF-β plus eupatilin were the same. RNA-seq analysis under the sequential stimulation condition was conducted using highly confluent cells, which could have affected the eupatilin-induced changes in gene expression. Gene Ontology analysis revealed that, under both stimulation conditions, the genes with the largest changes in expression encoded proteins classified as cellular components (7% and 20.5%, respectively), suggesting that eupatilin's MOA is related to its ability to induce morphological changes through its effect on cytoskeletal proteins. Specifically, eupatilin inhibited phosphorylation of Smad3 and rapidly depolymerized actin stress fibers. Smad3 positively regulates fibrogenesis *via* EMT [60]. These potential MOAs may have a potent effect on pathogenic myofibroblasts.

The CS is a hallmark of flavonoids. Our structure–function analysis suggested that specific carbon residues of the CS of eupatilin, as well as their linked functional groups, make essential contributions to antifibrotic activity. Therefore, modification of eupatilin *via* medicinal chemistry should be conducted cautiously to yield more efficacious derivatives. Our 14 day's oral gavage non-GLP toxicity study showed that eupatilin is a non-toxic drug administered into rats.

In conclusion, we discovered that a few CS-containing drugs, represented by eupatilin, can effectively curb lung fibrosis with no cellular toxicity, and that these drugs act directly on pathogenic myofibroblasts. We believe that eupatilin or its derivatives could be used for monotherapy of IPF; moreover, because the MOA of eupatilin is distinct from that of pirfenidone, combinatorial therapy could also be efficacious. Indeed, a synthetic analogue derived from eupatilin could attenuate the severity of IPF at even lower concentrations. Fig. 9 summarizes three potential MOAs that could give rise to the potent anti-IPF effect associated with eupatilin.

Funding

This study was supported by an intramural fund from Osteoneurogen, Inc..

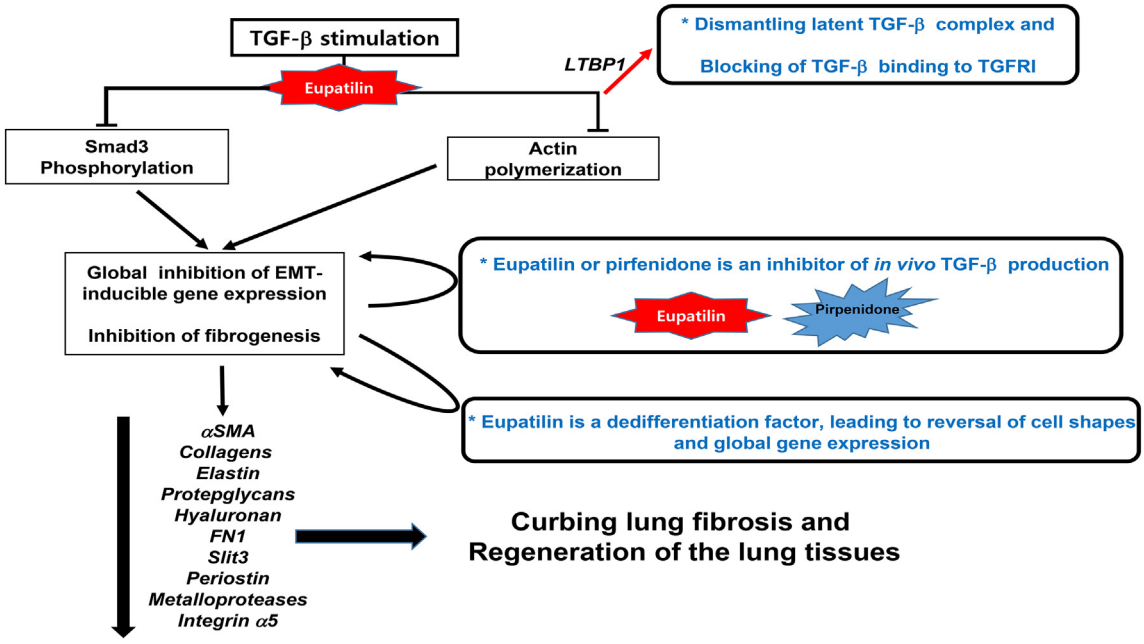

Fig. 9. Proposed MOAs of eupatilin, leading to anti-fibrotic capacity. Eupatilin directly acts on pathogenic myofibroblasts and inhibits fibrosis. Eupatilin rapidly depolymerizes actin stress fibers to which latent TGF-β complex is anchored. Under pathologic circumstances, the TGF-β cargo proteome, consisting of a heterodimeric integrin (mainly integrin *avβ3*) loaded with RGD, LAP1, and LTBP1, carry on the processed and active TGF-β and is relayed to TGFR. LTBP1 is secreted into the ECM. Upon actin depolymerization, latent TGF-β complex is dismantled, leaving active TGF-β at the cargo proteome and nullifying its binding to TGFR1. By dephosphorylation of Smad3 induction of EMT master regulators such as Snail2 may not be made possible. Eupatilin causes myofibroblasts to revert to HSC-like intermediate cell types. Whether actin depolymerization is responsible for this dedifferentiation remains to be scrutinized. Finally, eupatilin, like pirfenidone, inhibits *in vivo* TGF-β production.

Author contributions

B-S Youn and H- Kim conceived the idea. I–H Kim coordinated the experiments and helped to write the manuscript.; JY Lee contributed to real-time imaging; and Y-M Yoon took part in chemical screening and *in vitro* myofibroblast transdifferentiation assay. MK Maeng conducted phosphorylation analysis following eupatilin stimulation. TH Lee provide a consultation on oriental herbal medicines and their application to inflammation or fibrosis. JE Lee and Y E Park contributed significantly to protein identification and modeling of signaling pathways.

Competing financial interests

H-S Kim, I-H Kim and B-S Youn retain shares of Osteoneurogen, Inc. Y-M Yoon and MK Moon are employed by Osteoneurogen, Inc. A patent regarding anti-fibrosis and chromone scaffold has been granted by the Korean Intellectual Property Office. An international PCT and a US patent are being reviewed. The other authors have no conflict of interests.

Acknowledgments

The authors thank Prof. Ho-Sup Yoon (Nanyang Technological University, Singapore) for insightful comments on the manuscript.

Appendix A. Supplementary data

Supplementary data to this article can be found online at https://doi.org/10.1016/j.ebiom.2018.12.017.

References

[1] Bonnans C, Chou J, Werb Z. Remodelling the extracellular matrix in development and disease. Nat Rev Mol Cell Biol 2014;15(12):786–801.
[2] Stone RC, Pastar I, Ojeh N, et al. Epithelial-mesenchymal transition in tissue repair and fibrosis. Cell Tissue Res 2016;365(3):495–506.
[3] Meng XM, Nikolic-Paterson DJ, Lan HY. TGF-β: the master regulator of fibrosis. Nat Rev Nephrol 2016;12(6):325–38.
[4] Thomas BJ, Kan-O K, Loveland KL, Elias JA, Bardin PG. In the Shadow of Fibrosis: Innate Immune suppression Mediated by Transforming Growth Factor-β. Am J Respir Cell Mol Biol 2016;55(6):759–66.
[5] Chen Y, Ali T, Todorovic V, O'Leary JM, Kristina Downing A, Rifkin DB. Amino acid requirements for formation of the TGF-beta-latent TGF-beta binding protein complexes. J Mol Biol 2005;345(1):175–86.
[6] Fallowfield JA. Future mechanistic strategies for tackling fibrosis–an unmet need in liver disease. Clin Med (Lond) 2015;15(Suppl.(6):s83–7.
[7] Sgalla G, Cocconcelli E, Tonelli R, Richeldi L. Novel drug targets for idiopathic pulmonary fibrosis. Expert Rev Respir Med 2016;26:1–13.
[8] King CS, Nathan SD. Practical considerations in the pharmacologic treatment of idiopathic pulmonary fibrosis. Curr Opin Pulm Med 2015;21(5):479–89.
[9] Knüppel L, Ishikawa Y, Aichler M, et al. A novel antifibrotic mechanism of nintedanib and pirfenidone. Inhibition of collagen fibril assembly. Am J Respir Cell Mol Biol 2017;57(1):77–90.
[10] Rangarajan S, Kurundkar A, Kurundkar D, et al. Novel Mechanisms for the Antifibrotic Action of Nintedanib. Am J Respir Cell Mol Biol 2016;54(1):51–9.
[11] Dixon RA, Pasinetti GM. Flavonoids and isoflavonoids: from plant biology to agriculture and neuroscience. Plant Physiol 2010;154(2):453–7.
[12] Stapleton AE, Walbot V. Flavonoids can protect maize DNA from the induction of ultraviolet radiation damage. Plant Physiol 1994;105(3):881–9.
[13] Cheynier V, Comte G, Davies KM, Lattanzio V, Martens S. Plant phenolics: recent advances on their biosynthesis, genetics, and ecophysiology. Plant Physiol Biochem 2013;72:1–20.
[14] Fischer N, Seo EJ, Efferth T. Prevention from radiation damage by natural products. Phytomedicine 2018;47:192–200.
[15] Leyva-López N, Gutierrez-Grijalva EP, Ambriz-Perez DL, Heredia JB. Flavonoids as cytokine modulators: a possible therapy for inflammation-related diseases. Int J Mol Sci 2016;17(6):921.
[16] Emami S, Ghanbarimasir Z. Recent advances of chroman-4-one derivatives: synthetic approaches and bioactivities. Eur J Med Chem 2015;93:539–63.
[17] Gacche RN, Meshram RJ, Shegokar HD, et al. Flavonoids as a scaffold for development of novel anti-angiogenic agents: An experimental and computational enquiry. Arch Biochem Biophys 2015;577–578:35–48.
[18] Kim JY, Lee MS, Baek JM, Park J, Youn BS, Oh J. Massive elimination of multinucleated osteoclasts by eupatilin is due to dual inhibition of transcription and cytoskeletal rearrangement. Bone Rep 2015;3:83–94.
[19] Trapnell C, Roberts A, Goff L, et al. Differential gene and transcript expression analysis of RNA-seq experiments with TopHat and Cufflinks. Nat Protoc 2012;7(3):562–78.
[20] Sun J, Nishiyama T, Shimizu K, Kadota K. TCC: an R package for comparing tag count data with robust normalization strategies. BMC Bioinformatics 2013;14:219.
[21] Szklarczyk D, Franceschini A, Kuhn M, et al. The STRING database in 2011: functional interaction networks of proteins, globally integrated and scored. Nucleic Acids Res 2011;39:D561–8.
[22] Gabele E, Brenner DA, Rippe RA. Liver fibrosis: signals leading to the amplification of the fibrogenic hepatic stellate cell. Front Biosci 2003;8:d69–77.

[23] Terai S, Fushida S, Tsukada T, et al. Bone marrow derived "fibrocytes" contribute to tumor proliferation and fibrosis in gastric cancer. Gastric Cancer 2015;18(2):306–13.
[24] Piera-Velazquez S, Mendoza FA, Jimenez SA. Endothelial to mesenchymal transition (EndoMT) in the pathogenesis of human fibrotic diseases. J Clin Med 2018;5(4):45.
[25] Tennakoon AH, Izawa T, Kuwamura M, Yamate J. Pathogenesis of Type 2 Epithelial to Mesenchymal transition (EMT) in Renal and Hepatic Fibrosis. J Clin Med 2015;5(1):E4.
[26] Chen DQ, Feng YL, Cao G, Zhao YY. Natural Products as a source for Antifibrosis Therapy. Trends Pharmacol Sci 2018;39(11):937–52.
[27] Huang SK, Scruggs AM, McEachin RC, White ES, Peters-Golden M. Lung fibroblasts from patients with idiopathic pulmonary fibrosis exhibit genome-wide differences in DNA methylation compared to fibroblasts from nonfibrotic lung. PLoS One 2014;12(9):e107055.
[28] Morra L, Moch H. Periostin expression and epithelial-mesenchymal transition in cancer: a review and an update. Virchows Arch 2011;459(5):465–75.
[29] Wu Q, Hou X, Xia J, et al. Emerging roles of PDGF-D in EMT progression during tumorigenesis. Cancer Treat Rev 2013;39(6):640–6.
[30] Chen T, You Y, Jiang H, Wang ZZ. Epithelial-mesenchymal transition (EMT): A biological process in the development, stem cell differentiation, and tumorigenesis. J Cell Physiol;232(12):3261–3272.
[31] Kasai H, Allen JT, Mason RM, Kamimura T, Zhang Z. TGF-beta1 induces human alveolar epithelial to mesenchymal cell transition (EMT). Respir Res 2005;6:56.
[32] Wollin L, Wex E, Pautsch A, et al. Mode of action of nintedanib in the treatment of idiopathic pulmonary fibrosis. Eur Respir J 2015;45(5):1434–45.
[33] Xie L, Law BK, Chytil AM, Brown KA, Aakre ME, Moses HL. Activation of the Erk pathway is required for TGF-β1-induced EMT *in vitro*. Neoplasia 2004;6(5):603–10.
[34] Willis BC, Borok Z. TGF-beta-induced EMT: mechanisms and implications for fibrotic lung disease. Am J Physiol Lung Cell Mol Physiol 2007;293(3):L525–34.
[35] Robertson IB, Horiguchi M, Zilberberg L, Dabovic B, Hadjiolova K, Rifkin DB. Latent TGF-β-binding proteins. Matrix Biol 2015;47:44–53.
[36] Swaminathan V, Kalappurakkal JM, Mehta SB, et al. Actin retrograde flow actively aligns and orients ligand-engaged integrins in focal adhesions. Proc Natl Acad Sci U S A 2017;114(40):10648–53.
[37] Wu Y, Liu X, Zhou Q, et al. Silent information regulator 1 (SIRT1) ameliorates liver fibrosis via promoting activated stellate cell apoptosis and reversion. Toxicol Appl Pharmacol 2015;289(2):163–76.
[38] Chen DQ, Feng YL, Cao G, Zhao YY. Natural Products as a source for Antifibrosis Therapy. Trends Pharmacol Sci 2018;39(11):937–52.
[39] Wynn TA. Cellular and molecular mechanisms of fibrosis. J Pathol 2008;214(2):199–210.
[40] Ji HY, Lee HW, Shim HJ, Kim SH, Kim WB, Lee HS. Metabolism of eupatilin in rats using liquid chromatography/electrospray mass spectrometry. Biomed Chromatogr 2004;18(3):173–7.
[41] Strauss JF, Barbieri RL. Yen & Jaffe's Reproductive Endocrinology : Physiology, Pathophysiology, and Clinical Management. 7th. EdPhiladelphia: Elsevier Saunders; 2014.
[42] Verma N, Kumar P, Mitra S, et al. Drug idiosyncrasy due to pirfenidone presenting as acute liver failure: Case report and mini-review of the literature. Hepatol Commun 2017;2(2):142–7.
[43] Dong Y, Geng Y, Li L, et al. Blocking follistatin-like 1 attenuates bleomycin-induced pulmonary fibrosis in mice. J Exp Med 2015;212(2):235–52.
[44] Nakayama M, Nakajima D, Nagase T, Nomura N, Seki N, Ohara O. Identification of high-molecular-weight proteins with multiple EGF-like motifs by motif-trap screening. Genomics 1998;51(1):27–34.
[45] van der Slot AJ, Zuurmond AM, Bardoel AF, et al. Identification of PLOD2 as telopeptide lysyl hydroxylase, an important enzyme in fibrosis. J Biol Chem 2003;278(42):40967–72.
[46] Xiao H, Zeng J, Li H, et al. MiR-1 downregulation correlates with poor survival in clear cell renal cell carcinoma where it interferes with cell cycle regulation and metastasis. Oncotarget 2015;6(15):13201–15.
[47] Zepp JA, Zacharias WJ, Frank DB, et al. Distinct mesenchymal lineages and niches promote epithelial self-renewal and myofibrogenesis in the lung. Cell Rep 2017;170(6):1134–48.
[48] Vignozzi L, Morelli A, Cellai I, et al. J Steroid Biochem Mol Biol;165(B):277–92; 2017.
[49] Raghu G. Pharmacotherapy for idiopathic pulmonary fibrosis: current landscape and future potential. Eur Respir Rev 2017;26:170071.
[50] Raghu G, Brown KK, Collard HR, et al. Efficacy of simtuzumab versus placebo in patients with idiopathic pulmonary fibrosis: a randomised, double-blind, controlled, phase 2 trial. Lancet Respir Med 2017;5(1):22–32.
[51] Flaherty KR, Fell CD, Huggins JT, et al. Safety of nintedanib added to pirfenidone treatment for idiopathic pulmonary fibrosis. Eur Respir J 2018;52:1800230.
[52] Margaritopoulos GA, Vasarmidi E, Antoniou KM. Pirfenidone in the treatment of idiopathic pulmonary fibrosis: an evidence-based review of its place in therapy. Core Evid 2016;11:11–22.
[53] Lamouille S, Xu J, Derynck R. Molecular mechanisms of epithelial-mesenchymal transition. Nat Rev Mol Cell Biol 2014;15(3):178–96.
[54] Comeglio P, Filippi S, Sarchielli E, et al. Anti-fibrotic effects of chronic treatment with the selective FXR agonist obeticholic acid in the bleomycin-induced rat model of pulmonary fibrosis. J Steroid Biochem Mol Biol 2017;168:26–37.
[55] Kisseleva T, Cong M, Paik Y, et al. Myofibroblasts revert to an inactive phenotype during regression of liver fibrosis. Proc Natl Acad Sci U S A 2012;109(24):9448–53.
[56] Zhang H, Wu P, Chen F, et al. SILAC-based quantitative proteomic analysis of secretome between activated and reverted hepatic stellate cells. Proteomics 2014;14(17–18):1977–86.
[57] Ramachandran P, Iredale JP, Fallowfield JA. Resolution of liver fibrosis: basic mechanisms and clinical relevance. Semin Liver Dis 2015;35(2):119–31.
[58] Spagnolo P, Maher TM, Richeldi L. Idiopathic pulmonary fibrosis: recent advances on pharmacological therapy. Pharmacol Ther 2015;152:18–27.
[59] Piera-Velazquez S, Mendoza FA, Jimenez SA. Endothelial to Mesenchymal transition (EndoMT) in the Pathogenesis of Human Fibrotic Diseases. J Clin Med 2016;5(4):E45.
[60] Roberts AB, Tian F, Byfield SD, et al. Smad3 is key to TGF-beta-mediated epithelial-to-mesenchymal transition, fibrosis, tumor suppression and metastasis. Cytokine Growth Factor Rev 2006;17(1–2):19–27.